U.S. DEPARTMENT OF THE INTERIOR
U.S. GEOLOGICAL SURVEY

Use and Presentation of Magellan Quantitative Data in Venus Mapping

by

Bruce A. Campbell[1]

Open-File Report 95-519

This report is preliminary and has not been reviewed for conformity with U.S. Geological Survey editorial standards, or with the North American Stratigraphic Code. Any use of trade, product, or firm names is for descriptive purposes only and does not imply endorsement by the U.S. Government.

[1] Center for Earth & Planetary Studies, MRC 315, Smithsonian Institution, Washington, DC 20560

Table of Contents

List of Illustrations

List of Tables

I. Introduction

This report is a guide to possible uses for Magellan data within the context of Venus mapping. The goal is to provide a set of "cookbook" approaches which may allow mappers working over a broad range of viewing geometries to clearly communicate the surface properties of their units to a wide audience, with due care given to the ambiguities which can enter into such techniques. Backscatter coefficients and ancillary data (emissivity, topography, rms slope, and reflectivity) for Venus obtained by Magellan provide a unique view of the surface roughness at a variety of scales and the dielectric properties of the terrain. The active illumination and control of incidence angles afforded by the radar instrument also create a dataset having quantitative properties that can be compared with observations of potential terrestrial analog surfaces. In preparing a Venus map, it is thus valuable to the mapper and the reader to provide a distillation and interpretation of the quantitative properties of geologic units from the measurements available.

A set of presentation methods are shown, some of which are offered as standards for the use of quantitative data in map texts and figures. Many of the topics covered here are introduced in The Venus Geologic Mappers' Handbook [Tanaka et al., 1994] and this paper expands on these issues with information gained during analysis of Magellan data. One of the primary motivations of this paper is to archive equations and tables needed for Magellan data processing and to provide rationales for the importance of each dataset to future mappers and map users.

II. Radar Backscatter Cross Section

Radar backscatter cross section is defined as the area (meters squared) of an isotropic scatterer which would be required to return the observed echo power after adjustments for range, antenna gain, and other systematic variables. A more useful quantity is obtained by dividing this value by the area of the observed terrain, which varies somewhat from the true ground area due to the foreshortening effect of side-looking radar systems. The backscatter cross section per unit area is thus a dimensionless quantity which can be treated as an intrinsic property of the surface at a given wavelength, polarization, and incidence angle. The correct term for this value is backscatter

coefficient, but several other terms appear in published papers: sigma zero, specific backscatter cross section, absolute backscatter cross section, or simply the radar cross section. Magellan measurements are corrected to the dimensionless quantity during processing, as are the aircraft data used as planetary analogs.

The backscatter values on a Magellan CD-ROM image (or USGS quadrangle) have been scaled using an empirical model for radar echoes from Venus derived by Muhleman [1964]. The Muhleman law is a best-fit approximation to the average backscatter as a function of incidence angle which incorporates both the quasi-specular and diffuse components, treated separately elsewhere [Hagfors, 1967; 1970]. This scaling allows the dynamic range of the data to be compressed into the 8-bit format of the pixels, regardless of the incidence angle of the observations. The normalization also means that the gray-scale brightness of regions widely separated in latitude (assuming the left-looking angle profile) cannot be compared, because the incidence angles of the two observations will be different. In such cases we are looking at changes with respect to the Muhleman function, not variations in the true radar backscatter coefficient. Additional right-looking and stereo images were collected at a smaller range of incidence angles, but the coverage of these images is limited.

The first step in carrying out quantitative comparisons between map units is to find the backscatter coefficient (σ_o) from the raw image data. Given the DN (digital number) value of a pixel and its incidence angle, ϕ, we can use

$$\sigma_o = 10^{0.1[-20+(DN-1)/5]} \frac{0.0118 \cos(\phi+0.5)}{[\sin(\phi+0.5)+0.111 \cos(\phi+0.5)]^3} \quad (1)$$

where the half-degree shift in incidence angle was added inadvertently during data processing [Saunders et al., 1992]. If only the value in decibels relative to the Muhleman law is desired, then the equation is

$$\sigma_o = -20 + (DN-1)/5 \quad (2)$$

The incidence angle is dependent upon the latitude of the target and the type of observation (left-looking, right-looking, stereo, or the special Maxwell geometry; fig. 1). Incidence angle values and Muhleman law correction factors for the four incidence angle modes as a function of latitude

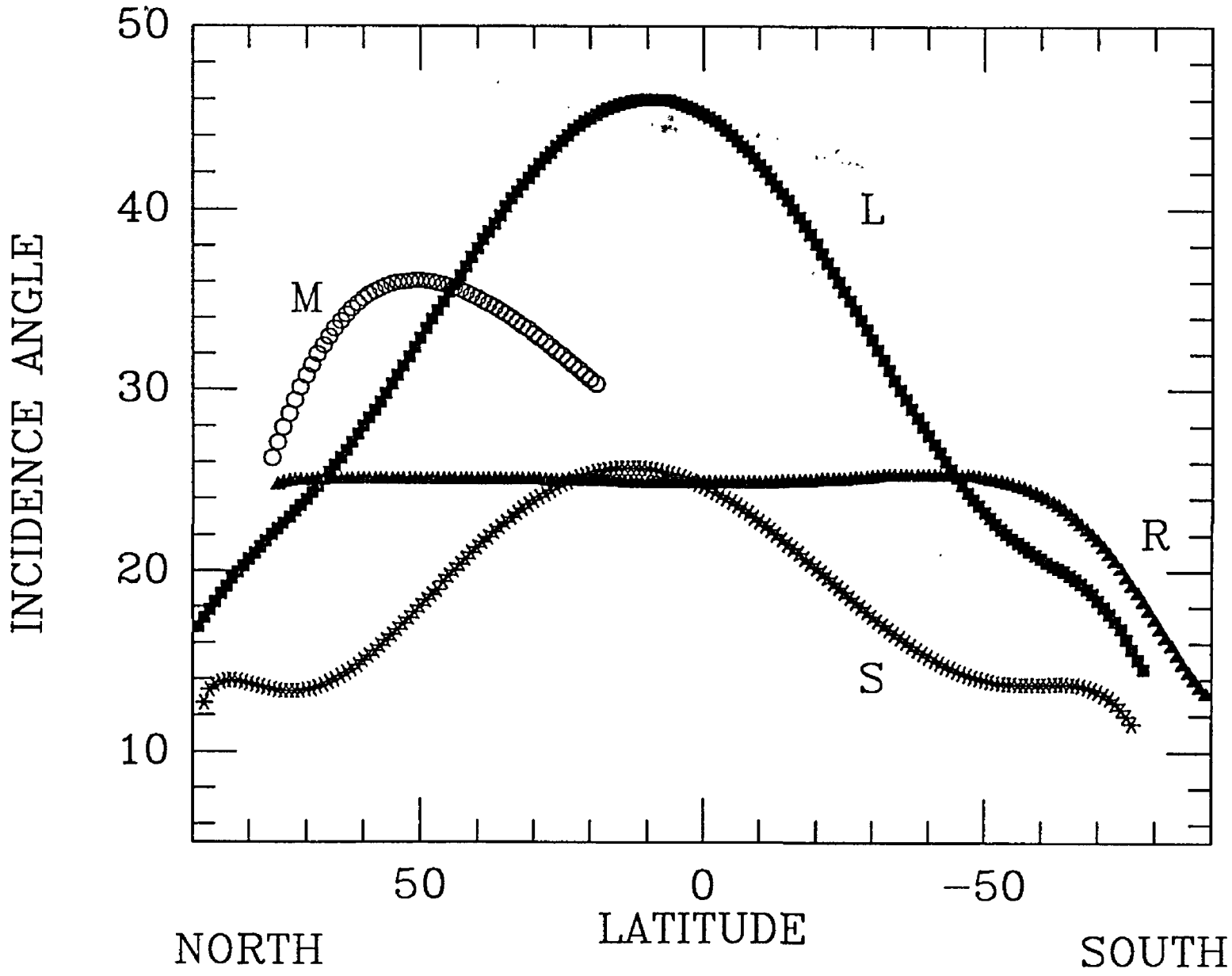

Figure 1. Radar incidence angle versus latitude for four viewing geometry profiles used during the Magellan mission (table 1). Left-looking (L), right-looking (R), Maxwell left-looking stereo (M), and Cycle 3 left-looking stereo (S) profiles labeled. Actual surface coverage for each profile varies widely.

on Venus are listed in table 1A-D. Backscatter coefficients are often presented in logarithmic form (value in decibels=10 $\log_{10} \sigma_o$) due to their wide dynamic range; equation (2) and table 1 provide a means for deriving this coefficient in decibels for any single Magellan image pixel.

Any averaging of pixels within Magellan images must be carried out with σ_o values in the "linear" format above (eq 1). This method was used to produce the C-MIDR files from the original full-resolution (F-BIDR) maps. Significant errors may occur if DN values are averaged prior to rescaling. The reason for averaging in power rather than in logarithmic representation is that the radar echo from a low-resolution image cell generally equals the sum of the power from each of the constituent higher resolution pixels (that is, the scattering process is incoherent from one 75-m area to the next). Energy is conserved in this averaging process but not in calculating the mean of the DN distribution. In order to average over extended areas, you will need software that determines the incidence angle of the pixel, calculates σ_o from the DN value, and averages the measurements within a sample area. Appendix 1 describes a Fortran program (**mgn_data**) available over the Internet which will perform this averaging on Magellan image files. Appendix 2 discusses a program (**anc_data**) that can be used to obtain emissivity, topography, rms slope, and reflectivity averages for any given latitude, longitude box.

III. Comparison of σ_o Among Map Units and with Terrestrial Analogs

The backscatter coefficient of a surface changes with the wavelength, polarization, and incidence angle of the radar energy. The magnitude of the echo and the variation in the return with changes in the above parameters can be linked to surface roughness, to the bulk dielectric constant of the material, and occasionally to subsurface scattering when the dielectric losses in the material are low. Surface roughness can in turn be treated as a combination of scatterers at a wide range of spatial scales, whose effect on the backscatter varies. Therefore, numerous possible explanations exist for variations in backscatter; however, we can make some general statements based on terrestrial radar studies.

ROCKY SURFACES (THOSE HAVING NO SOIL COVER): At incidence angles >30°, the changes in HH (horizontal transmit, horizontal receive) backscatter coefficient are directly correlated with roughness at the scale of the wavelength and the bulk dielectric constant of the surface. The effect of the two changes is illustrated in figure 2 with results from Hawaii. This plot shows that changes in wavelength-scale roughness will likely be the dominant cause of radar brightness variations in areas of Venus where the dielectric constant is <10 (that is, everywhere below about 6,053 km in planetary radius). Values of 8-9 are the maximum found for terrestrial dense basalt samples.

At incidence angles near or below 30°, the HH backscatter cross section may not represent the wavelength-scale roughness of the surface, because large "quasi-specular" facets begin to play a role in the measured echo. For terrestrial lava flows, this can lead to a complete loss of roughness discrimination or contrast reversals between smooth and rough terrain at angles of 20-30°. Dielectric effects are similar to those seen at more oblique angles, in that we expect a linear variation in backscatter with changes in the Fresnel reflectivity. This loss in discrimination, for lava flows on Kilauea, is shown on figure 3. In using the Magellan images at these incidence angles, one can expect that many lava flow fields will appear rather featureless relative to those viewed at more oblique angles.

SURFACES HAVING A POROUS COVERING: At all incidence angles, the backscatter cross section will drop as a result of attenuation by loose mantling material. The average dielectric constant will also fall if the soil is simply a less dense version of the base rock (see the emissivity sections below). If the soil is deep (>1 m), has a low loss factor, and contains wavelength-size rocks, the observed backscatter could be much higher than that of a solid smooth surface having the same population of rocks per unit area. Such deep-soil scenarios do not seem likely on Venus (although they are common on the Moon), but shallow soils almost certainly occur in some areas. An estimate of the amount of loss within soils can be obtained using equations found in Ulaby et al. [1987, p. 67, 847]. For two-way passage through a layer, the power (P) lost due to attenuation will be

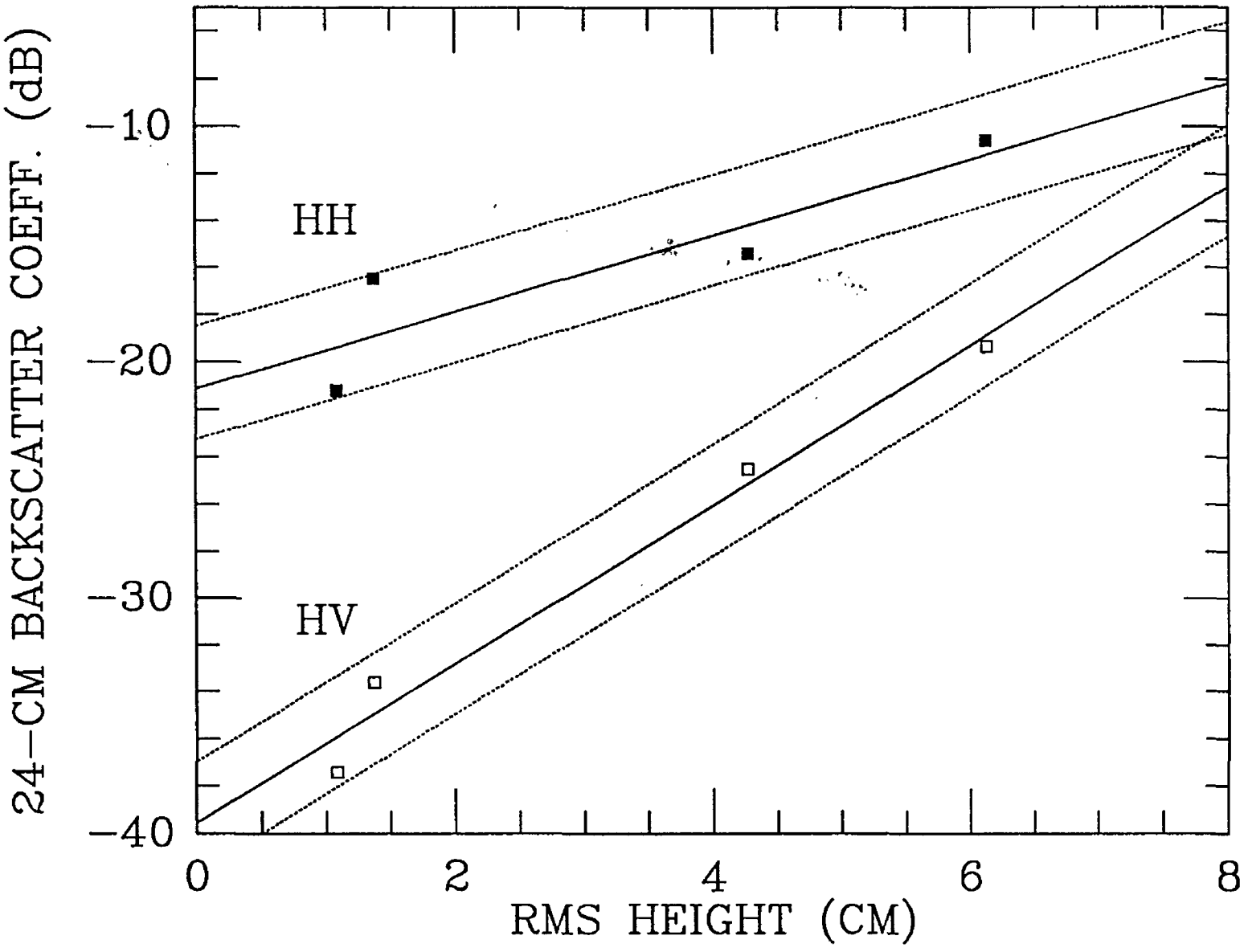

Figure 2. HH (horizontal transmit, horizontal receive) and HV (horizontal transmit, vertical receive) backscatter coefficients versus root mean square (rms) height for four lava flows in Hawaii. Radar data are average 24-cm wavelength echoes at incidence angles of 30-45°. The rms heights were calculated from 5- to 8-m profiles with 5-cm sample spacing, filtered using a highpass cutoff of 1 m to suppress large-scale topography. Solid lines are best fits to data points. If we assume the mean dielectric constant of these lavas is 5, then we can calculate the shift in echo power due to changes in the dielectric constant. Dotted lines show the modified best-fit line for dielectric values of 10 and 3. Data from other sources show 24-cm HH and HV echoes for these flows remain nearly constant for rms heights greater than 10 cm.

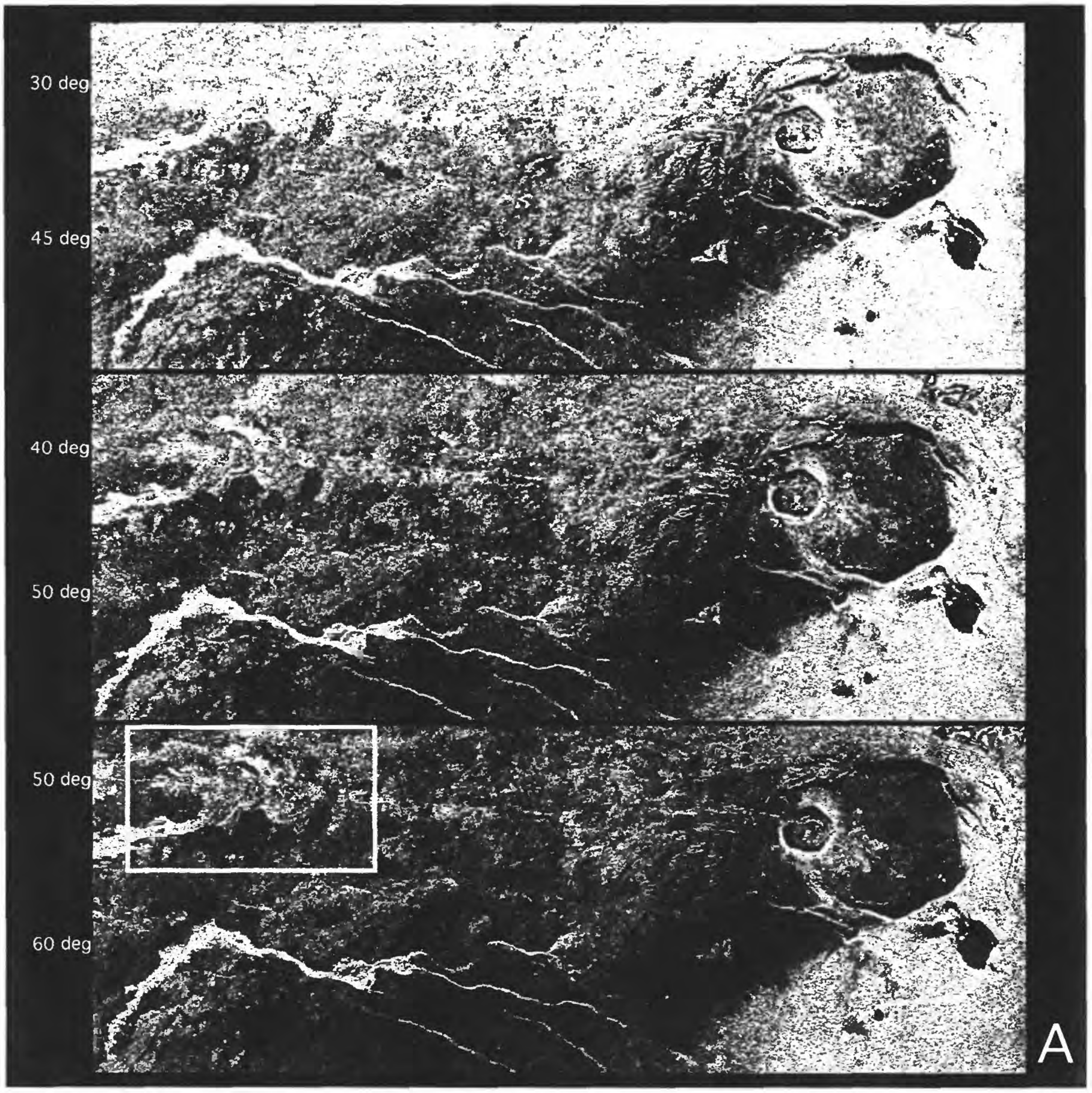

Figure 3. L-band (24 cm) HH-polarization (A) and HV-polarization (B) radar images of Kilauea and the Kau desert collected at three viewing geometries, rectified to a uniform 10 m pixel size. Incidence angles are marked along left side of each image. Of particular interest is Mauna Iki volcanic shield in the upper left of each frame, opposite incidence angle label (marked by a white box in the lower image of A). At high angles (>30 deg), flows from Mauna Iki are distinct from one another in HH images. whereas at lower angles there is little separation between pahoehoe and a'a surface textures. Compare this with the high degree of unit discrimination possible at all angles with the HV images.

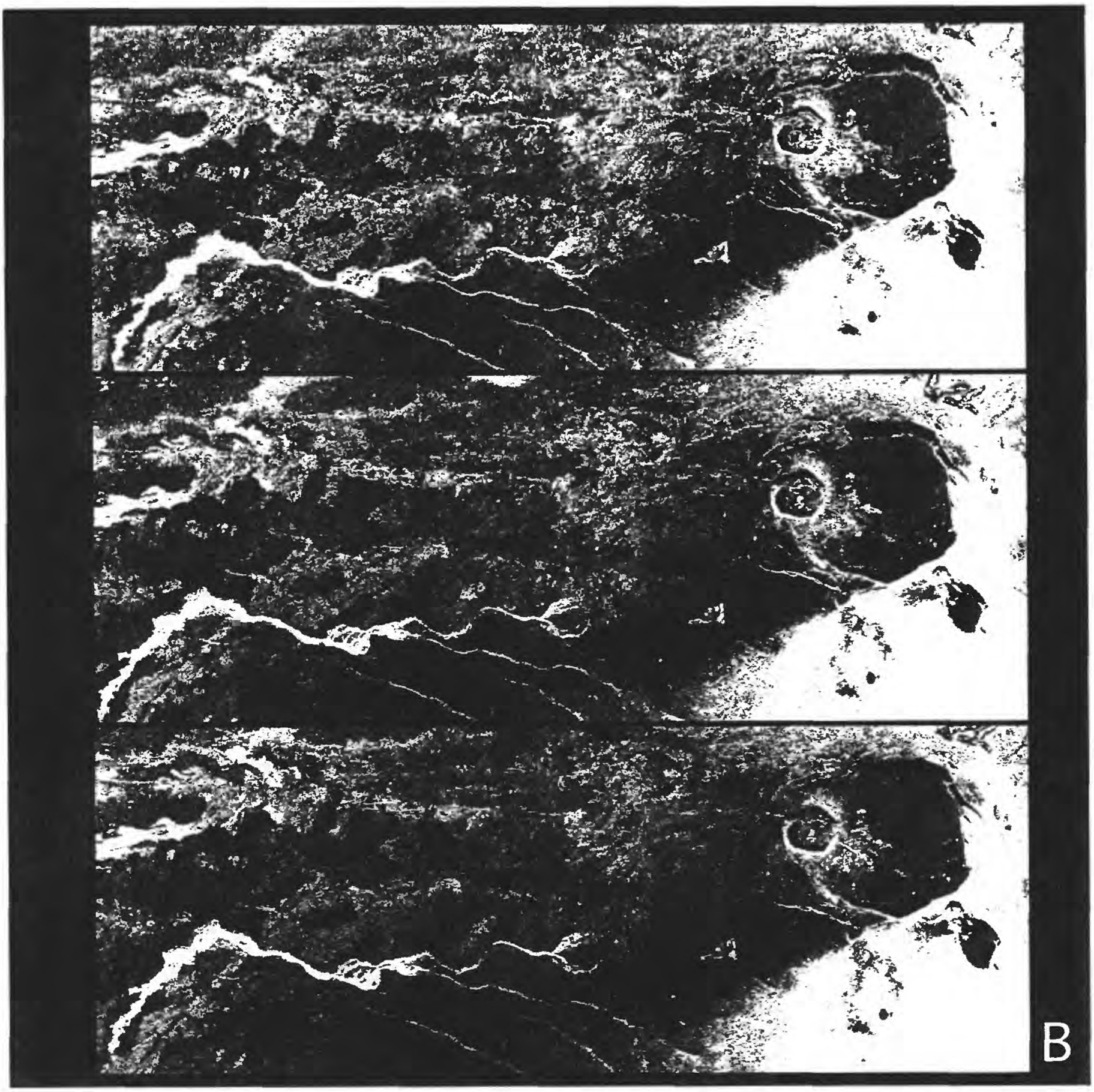

Figure 3. L-band (24 cm) HH-polarization (A) and HV-polarization (B) radar images of Kilauea and the Kau desert collected at three viewing geometries, rectified to a uniform 10 m pixel size. Incidence angles are marked along left side of each image. Of particular interest is Mauna Iki volcanic shield in the upper left of each frame, opposite incidence angle label (marked by a white box in the lower image of A). At high angles (>30 deg), flows from Mauna Iki are distinct from one another in HH images, whereas at lower angles there is little separation between pahoehoe and a'a surface textures. Compare this with the high degree of unit discrimination possible at all angles with the HV images.

$$\frac{P_{out}}{P_{in}} = \exp\left(-\frac{8\pi h}{\lambda \cos\phi}\sqrt{\frac{\varepsilon}{2}\left[\sqrt{1+\tan^2\delta}-1\right]}\right) \quad (3)$$

where h is the layer depth, λ is the radar wavelength in vacuum (12.6 cm for Magellan), ε is the real part of the soil dielectric constant, ϕ is the incidence angle in the soil (after refraction), and $\tan\delta$ is the microwave "loss tangent" of the soil. Loss tangent is the ratio of the imaginary and real parts of the complex dielectric constant, and typical values for dry lunar soil at radar wavelengths are 0.002 to 0.02. This equation can provide an estimate of the depth of a mantling layer if there is a good estimate of the backscatter coefficient of an unmantled surface (for example, a lava flow which is partially covered by fine crater ejecta [see Campbell et al., 1992]).

PRESENTATION OF DATA: What does this mean for mapping conventions? There are clearly problems in trying to make comparisons between rock units seen at widely varying geometries, and mappers working with data at smaller incidence angles can expect to see a diminished dynamic range between rough and smooth surfaces. Rather than try to force a set of interpretive conventions on everyone, a radar correlation chart may be produced, which presents the mean backscatter properties of various units in comparison to the Venus average and selected terrestrial analog terrains. Sources for these comparative values can be found in Plaut [1991], Arvidson et al. [1992], Campbell and Campbell [1992], and Gaddis [1992]. A sample plot of this type is shown in figure 4, where scales in angle and cross section are recommended as a template for use on Venus maps. When multiple-angle data are available, units can have a portion of their backscatter function plotted on this diagram. The correlation chart serves the dual purpose of helping the mapper make informed judgements as to what are real changes in surface roughness within their areas (versus the subjective effects of image contrast stretching) and provides readers with a means to extrapolate results from one map to another at their own peril.

The radar backscatter coefficients for the Hawaiian lava flows and the Muhleman scattering law used in figure 4 are available as ascii data files over the Internet (app. 3), and it is suggested that all correlation charts use at least these comparison curves. If the radar behavior of other terrestrial

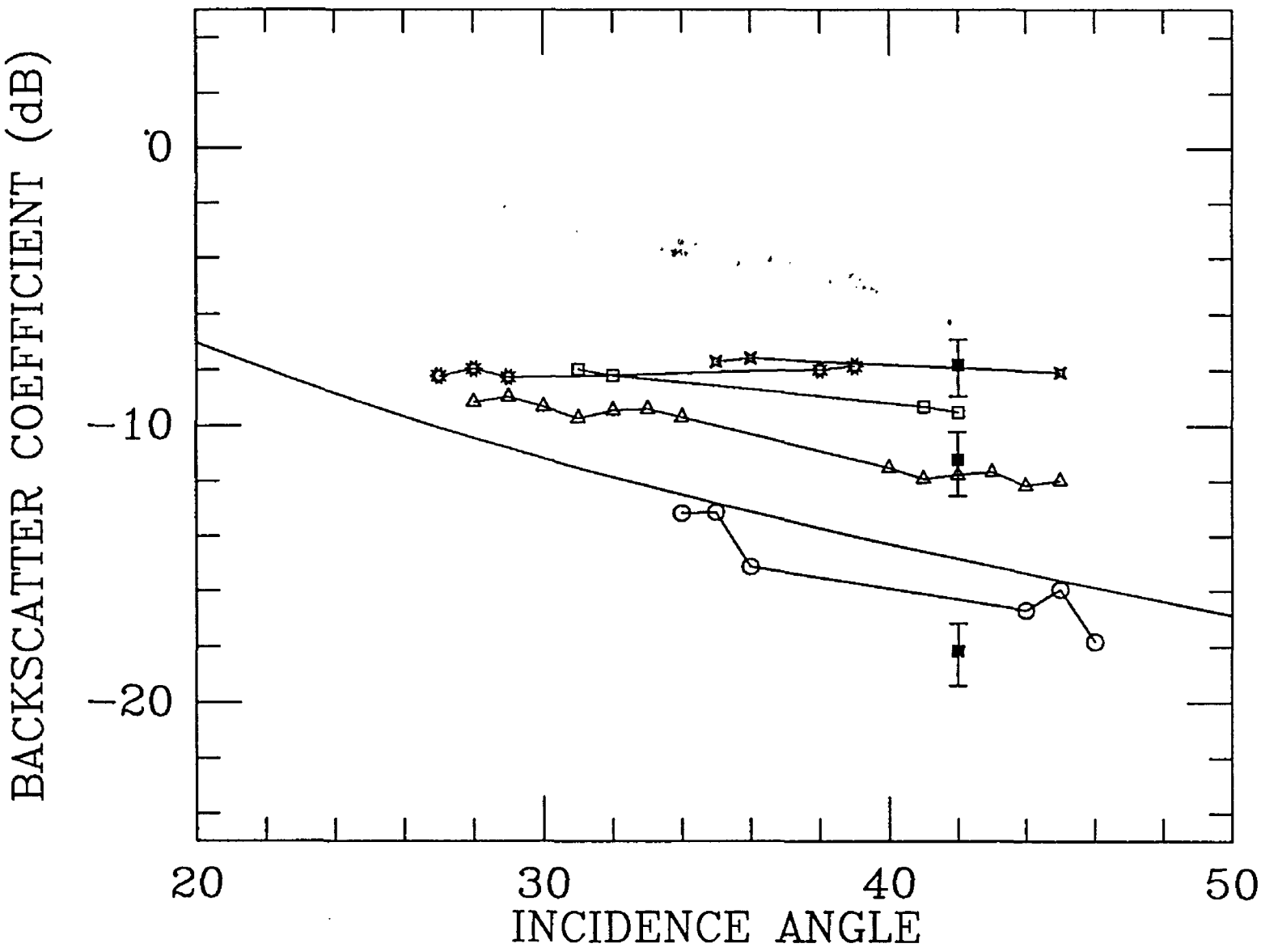

Figure 4. Example radar correlation chart. Connected plot symbols are for five lava flows on Kilauea, with roughnesses that extend from very smooth pahoehoe to jagged, spiny a'a [Campbell and Campbell, 1992]. Solid line is average scattering law for Venus defined by Muhleman [1964]. Three points shown with error bars are selected Venus sample areas listed in table 2.

terrains is needed to illustrate unit properties (for example, echoes from silicic domes or dry soil layers), mappers should feel free to add them to the diagram. The 12.6-cm (S-band) lava flow echoes shown were interpolated from 6-cm (C-band) and 24-cm (L-band) AIRSAR data using the relationship

$$\sigma_o^s = 0.377\ \sigma_o^l + 0.623\ \sigma_o^c \qquad (4)$$

The unit description should contain only the data product from which the backscatter information was obtained (for example, C1-30n045) and the latitude and longitude boundaries of the example site (pixel values within an image should not be used, since the reader may wish to examine the site using a different product). Actual values of backscatter coefficient and other parameters (emissivity, rms slope, Fresnel reflectivity, and elevation) should be placed in tables on the map sheet. For any given unit, the mapper should provide the mean, standard deviation, pixel scale, and the number of samples used to find the backscatter coefficient of the example site. Situations may arise where the standard deviation of the backscatter data is larger than the mean value, which may indicate a poorly chosen or very small test site that has widely varying brightness or a skewed probability distribution.

A single example area may not represent the full range of behavior within a given terrain unit, such as a volcano with interfingered bright and dark lava fields. If the mapper feels that the range of backscatter is significant, two averages could be quoted to illustrate the variation in properties across the unit. Map reviewers will need to check the selection and description of these example sites to ensure consistency. The interpretation section of the unit label should include a discussion of the significance of these results to the nature of the unit, particularly where surface properties appear to diverge significantly from the average behavior. An example data table corresponding to the Venus sample sites plotted in figure 4 is shown in table 2; all of these data were produced using the two programs (**mgn_data** and **anc_data**) discussed in the appendixes.

IV. Interpretation of Emissivity Data

Magellan collected measurements of the passive thermal emission from the surface of Venus at the same wavelength (12.6 cm) and viewing geometry as the synthetic aperture radar (SAR) [Pettengill

et al., 1992]. These data have a low spatial resolution (20-90 km) but provide a useful guide to the dielectric properties (and thus the density or metallic mineral content) of the surface. Maps of the horizontal-polarized emissivity, E_h, resampled to a 4.6-km grid size, are on the GxDR CD-ROMS. It should be kept in mind that these maps are assembled using a weighted average of measurements, so the specific value of E_h at a given point on the ground should not be taken as precise. The original footprint values can be read from the ARCDR CD-ROMS by using the MGMDQE program available over Internet from MIT (app. 4).

If a surface is perfectly smooth, the emissivity will be the complement of the Fresnel reflection coefficient, R, for the same polarization and incidence angle (ϕ)

$$E(\phi) = 1 - R(\phi) \tag{5}$$

and the dielectric constant, ε, can be found (by iteration) from

$$E_h = \frac{\sin 2\phi \, \sin 2\theta}{\sin^2(\theta + \phi)} \tag{6}$$

$$E_v = \frac{\sin 2\phi \, \sin 2\theta}{\sin^2(\theta + \phi)\cos^2(\phi - \theta)} \tag{7}$$

$$\theta = \sin^{-1}\left(\frac{\sin\phi}{\sqrt{\varepsilon}}\right) \tag{8}$$

where the h and v subscripts refer to horizontal and vertical polarizations. It is important to note the difference between the viewing geometries of the radiometer (25-45°) and the altimeter (within 15° of nadir); the emissivity should not be treated as the complement of the nadir reflectivity.

Table 3 presents values of ε for a range of incidence angles and E_h assuming a plane interface, which may be used to estimate the dielectric constant of many plains surfaces to a reasonable accuracy. As the surface becomes rougher (either at tens of meters scale or at wavelength scale), the emissivity tends to pull toward the average of the values for the two polarizations above. If we assume that this average represents the emissivity of a completely rough surface, then a second estimate of the dielectric constant can be made which bounds the possible range for that terrain unit. These rough-surface dielectric values are also shown in table 3. Such estimates are not necessarily exact, because the rough-surface estimate is not rigorous and some areas may have a mixture of soil and rock. For the majority of surfaces to be mapped, however, these values are a

useful guide to the properties of the terrain [Campbell, 1994]. The emissivity and the smooth- and rough-surface estimates of dielectric constant should be provided as additional information for each major map unit; the program described in appendix 2 calculates these values. For all the ancillary data values derived from the GxDR files, no standard deviation should be quoted, as these values are weighted averages of the original footprint values and the degree of oversampling varies with location on the planet. The minimum and maximum of each parameter over a sample region may be of value, so these ranges are included in the **anc_data** output.

Terrestrial basalts have dielectric constants that depend largely on the rock density (fig. 5), with powders having values of ~2 and solid rocks reaching values of 9 [Ulaby et al., 1988]. Lava flows, crater ejecta blankets, highland areas, and plains on Venus all exhibit variability in their dielectric properties, possibly indicating changes in density, iron/titanium content, chemical alteration, post-emplacement formation of soil, or a combination of these factors. In the absence of other types of stratigraphic markers, these changes should be explored as possible clues to the emplacement history of the various deposits.

V. Interpretation of Reflectivity Data

The Magellan altimeter system measured backscattered energy within about 15° of the nadir. These echoes were used to estimate the surface elevation, Fresnel reflectivity, and rms slope by fitting "templates" based on the Hagfors scattering function to each group of returned pulses [Ford and Pettengill, 1992]. This model assumes a gently undulating surface with no wavelength-scale roughness. Natural surfaces generally depart from this assumption, so a correction is made to the reflectivity for diffuse scattering by wavelength-scale rocks. The resulting reflectivity estimate is related to the dielectric constant by

$$\rho = \left[(\sqrt{\varepsilon} - 1)/(\sqrt{\varepsilon} + 1)\right]^2 \tag{9}$$

$$\varepsilon = \left[\frac{1 + \sqrt{\rho}}{1 - \sqrt{\rho}}\right]^2 \tag{10}$$

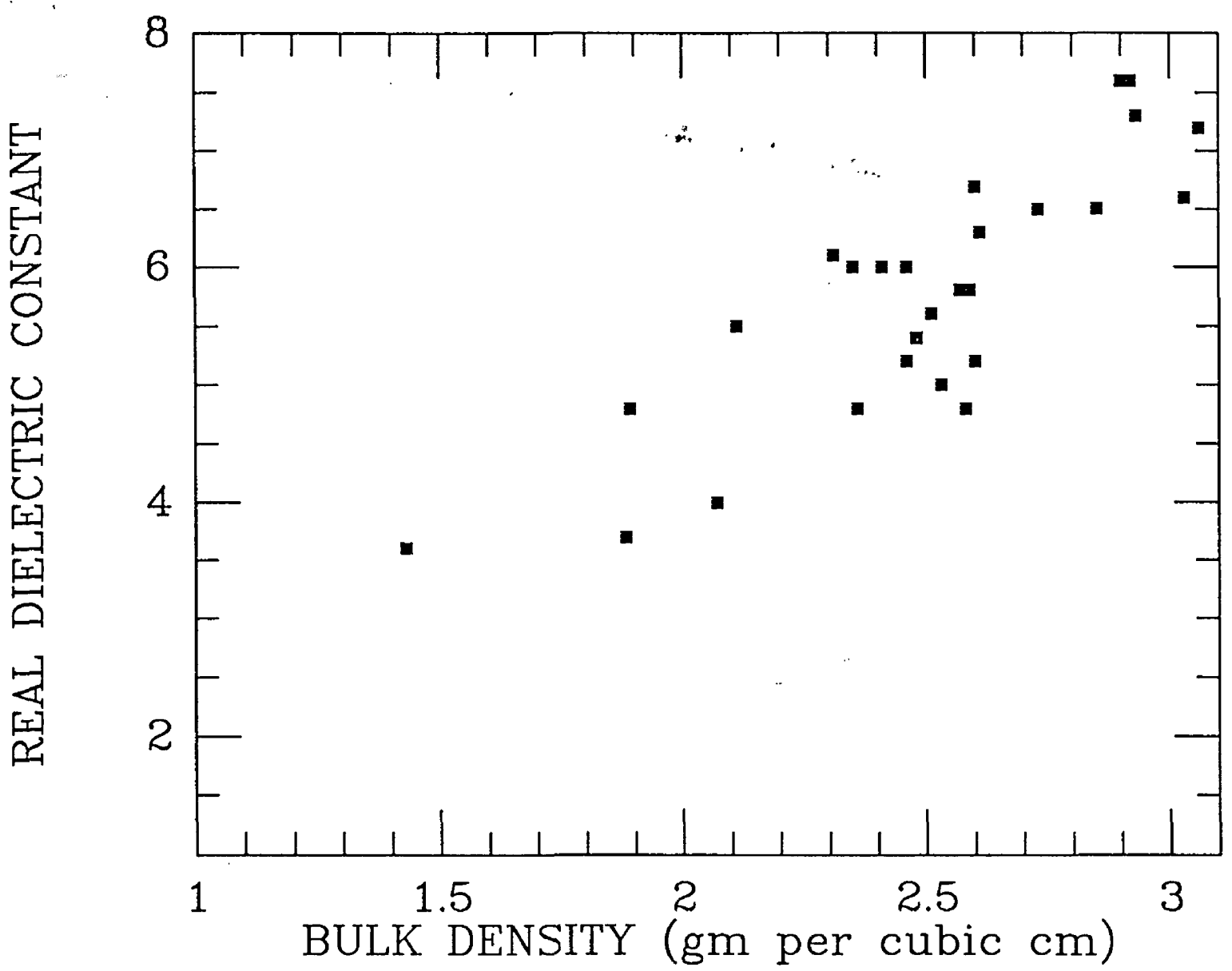

Figure 5. Real dielectric constant (ε) versus bulk density for terrestrial volcanic rocks (basalt, rhyolite, dacite, andesite, and diabase). Data from Ulaby et al. [1988].

For smooth areas, these results should be reasonably accurate. On rough terrain (tesserae, ridges, or rough lava flows), the Hagfors model is no longer applicable, and the reflectivity estimates should be treated with great caution even with the diffuse correction. As a comparison to values obtained from the emissivity, they should be discussed in the map analysis. Values for the dielectric constant versus Fresnel reflectivity are listed in table 4.

VI. Interpretation of RMS Slope Values

The rms slope value derived from the Hagfors model is an estimate of the slope distribution of the surface at scales of tens to hundreds of meters. Comparisons of lunar photogrammetric data and radar echoes show some degree of correlation between the two methods of measuring slopes, but the baseline over which the radar results apply is often difficult to quantify [Moore et al., 1980]. For much of Venus, the Magellan rms slope values follow the trend of the SAR echoes, with rougher surfaces having higher slopes and higher σ_0. Comparing these data with terrestrial analog surfaces has not been simple, and numerous questions as to the derivation and interpretation of such slope estimates remain [Simpson and Tyler, 1982; McCollom and Jakosky, 1992; Campbell and Garvin, 1993]. Published maps produced by the Stanford research group [Tyler et al., 1992], using different techniques than those used to make the current GsDR dataset [Ford and Pettengill, 1992], suggest that the choice of data reduction technique may strongly affect the estimate of rms slope in rough areas. Rms slope is nonetheless a valuable measure of angular spreading in the near-nadir radar echo, which can be a useful diagnostic of inhomogeneity within the footprint or of possible porous terrain units [Campbell and Rogers, 1994]. The average value and range of this parameter, which are part of the **anc_data** output, should be included in the map unit description.

VII. Identification of Surficial Units in Ancillary Datasets

The definition of map units will likely be based almost entirely on the Magellan SAR images. However, some surficial materials, such as crater ejecta, are better delineated within emissivity

images than by their radar backscatter characteristics, and the use of these data for characterizing such materials is important. At least five types of surficial deposits can be suggested for possible mapping:

1. Low-dielectric (high emissivity) units associated with impact craters. These units appear to be deposits of fine-grained soil that may be several tens of centimeters deep. A type example is the ejecta from Annia Faustina, which blankets rough lava flows from Gula Mons [Campbell et al., 1992]. Evidence of mantling relations is sometimes vague, but careful mapping of such units may provide important clues to regional stratigraphy.

2. High-dielectric (low emissivity) units associated with impact craters. These units are typically seen as the parabolas, which have little or no SAR signature but a dramatic low emissivity relative to the plains, and in some crater floors. The parabolas likely are thin deposits of fine-grained material with a concentration of high-dielectric mineral or metal grains (perhaps produced by impact melting and recondensation). The high-dielectric crater floors are probably impact melt sheets.

3. Low-dielectric areas associated with volcanism. Type examples can be found on the north flanks of Maat Mons, where radar-dark material appears to mantle rough lava flows. Such deposits may have been produced by eruptions of pyroclastics or ignimbrites.

4. Low-dielectric areas in the plains and some upland areas. These areas are found in a variety of settings, some of which suggest that the emissivity anomaly is due to soil formation or accumulation of fine (impact?) material. In other areas the radar return is actually higher than the neighboring lower emissivity plains. Mapping of these features is needed to define their occurrences and probable modes of formation.

5. Surfaces in the highlands with very high dielectric constants. Though some lava flows and other features have dielectric constants as high as 9, the highlands surfaces (above ~6,053 km radius) may reach values of 50 or more. The mechanism by which this high dielectric constant is produced remains controversial [Pettengill et al., 1992; Shepard et al., 1994; Campbell, 1994; Brackett et al., 1995]. Given the range of behaviors and the obvious elevation dependence of the dielectric constant, these areas should be mapped as separate rock units only when boundaries are

apparent. High-pass filtering of the radar images has been shown to be a useful means for defining some rock or structural units in the high-dielectric areas.

VIII. Summary

This report presents a set of interpretive methods that form a template for the presentation of Magellan data on Venus geologic maps. It is suggested that mappers select type examples for most areally extensive units and that the data be presented in a table of properties and a radar correlation chart. Examples of these are shown here and a set of program tools are available, which should permit all of the mappers to produce the necessary values. These same programs may also allow reviewers to check the data on a map or to suggest alternative sample sites.

Acknowledgments

Helpful comments by Jeffrey Johnson, Henry Moore, Steve Saunders, Jim Zimbelman, and the Venus Mapping Steering Group are greatly appreciated.

References Cited

Arvidson, R.E., R. Greeley, M.C. Malin, R.S. Saunders, N. Izenberg, J.J. Plaut, E.R. Stofan, and M.K. Shepard, Surface modification of Venus as inferred from Magellan observations of plains, J. Geophys. Res., 97, 13303-13318, 1992.

Brackett, R.A., B. Fegley, and R.E. Arvidson, Volatile transport on Venus and amplications for surface geochmistry and geology, J. Geophys. Res., 100, 1553-1563, 1995.

Campbell, B.A., Merging Magellan emissivity and SAR data for analysis of Venus surface dielectric properties, Icarus, 112, 187-203, 1994.

Campbell, B.A., and P.G. Rogers, Bell Regio, Venus: Integration of remote sensing data and terrestrial analogs for geologic analysis, J. Geophys. Res., 99, 21153-21171, 1994.

Campbell, B.A., and J.B. Garvin, Lava flow topographic measurements for radar data interpretation, Geophys. Res. Letters, 20, 831-834, 1993.

Campbell, B.A., R.E. Arvidson, and M.K. Shepard, Radar polarization properties of volcanic and playa surfaces: Applications to terrestrial remote sensing and Venus data interpretation, J. Geophys, Res., 98, 17099-17113, 1993.

Campbell, B.A., and D.B. Campbell, Analysis of volcanic surface morphology on Venus from comparison of Arecibo, Magellan, and terrestrial airborne radar data, J. Geophys. Res., 97, 16,293-16,314, 1992.

Campbell, D.B., N.J.S. Stacy, W.I. Newman, R.E. Arvidson, E.M. Jones, G.S. Musser, A.Y. Roper, and C. Schaller, Magellan observations of extended impact crater related features on the surface of Venus, J. Geophys. Res., 97, 16,249-16,278, 1992.

Ford, P.G., and G.H. Pettengill, Venus topography and kilometer-scale slopes, J. Geophys. Res., 97, 13,102-13,114, 1992.

Gaddis, LR., Lava flow characterization at Pisgah volcanic field, California, with multi-parameter imaging radar, Geol. Soc. Am. Bull., 104, 695-703, 1992.

Hagfors, T., Remote probing of the Moon by infrared and microwave emissions and by radar, Radio Science, 5, 189-227, 1970.

Hagfors, T., A study of the depolarization of lunar radar echoes, Radio Science, 2, 445-465, 1967.

McCollom, T.M., and B.M. Jakosky, Interpretation of planetary radar observations: The relationship between actual and inferred slope distributions, J. Geophys. Res., 98, 1173-1184, 1992.

Moore, H.J., J.M. Boyce, G.G. Schaber, and D.H. Scott, Lunar remote sensing and measurements, USGS Prof. Paper 1046-B, 1980.

Muhleman, D.O., Radar scattering from Venus and the Moon, Astron. J., 69, 34-41, 1964.

Pettengill, G.H., P.G. Ford, and R.J. Wilt, Venus surface radiothermal emission as observed by Magellan, J. Geophys. Res., 97, 13,091-13,102, 1992.

Plaut, J.J., Radar scattering as a source of geological information on Venus and Earth, PhD dissertation, Washington Univ., St. Louis, 1991.

Saunders, R.S., et al., Magellan mission summary, J. Geophys. Res., 97, 13,067-13,090, 1992.

Shepard, M.K., R.E. Arvidson, R.A. Brackett, and B. Fegley, A ferroelectric model for the low emissivity highlands on Venus, Geophys. Res. Letters, 21, 469-472, 1994.

Simpson, R.A., and G.L. Tyler, Radar scattering laws for the lunar surface, IEEE Trans. Ant. Prop., 30, 438-449, 1982.

Tanaka, K.L. (compiler), The Venus geologic mappers' handbook, U.S.G.S. Open-file Report 94-438, 66 p., 1994.

Tyler, G.L., R.A. Simpson, M.J. Maurer, and E. Holmann, Scattering properties of the Venus surface: Preliminary results from Magellan, J. Geophys. Res., 97, 13115-13140, 1992.

Ulaby, F.T., T. Bengal, J. East, M.C. Dobson, J. Garvin, and D. Evans, Microwave dielectric spectrum of rocks, Rep. 23817-1-T, Univ. of Michigan Radiation lab, Ann Arbor, MI, 1988.

Ulaby, F.T., R.K. Moore, and A.K. Fung, Microwave Remote Sensing, Addison-Wesley, Reading, MA, 1987.

TABLE 1A. Venus latitude, left-looking incidence angle, and Muhleman correction in decibels. South latitudes are negative, north latitudes are positive.
[correction factor can be added to Magellan normalized cross section values to obtain backscatter coefficient σ_0].

Lat	Ang	Factor	Lat	Ang	Factor	Lat	Ang	Factor
-90	*****	******	-30	32.78	-14.28	30	42.10	-17.01
-89	*****	******	-29	33.34	-14.46	31	41.71	-16.91
-88	*****	******	-28	33.88	-14.63	32	41.33	-16.80
-87	*****	******	-27	34.42	-14.80	33	40.96	-16.70
-86	*****	******	-26	34.96	-14.96	34	40.60	-16.60
-85	*****	******	-25	35.48	-15.12	35	40.12	-16.47
-84	*****	******	-24	36.01	-15.28	36	39.64	-16.34
-83	*****	******	-23	36.53	-15.44	37	39.19	-16.21
-82	*****	******	-22	37.06	-15.60	38	38.76	-16.09
-81	*****	******	-21	37.59	-15.75	39	38.33	-15.97
-80	*****	******	-20	38.13	-15.91	40	37.85	-15.83
-79	*****	******	-19	38.65	-16.06	41	37.35	-15.68
-78	14.56	-6.37	-18	39.13	-16.19	42	36.85	-15.54
-77	15.11	-6.70	-17	39.56	-16.32	43	36.36	-15.39
-76	15.66	-7.02	-16	40.01	-16.44	44	35.88	-15.25
-75	16.23	-7.34	-15	40.50	-16.58	45	35.40	-15.10
-74	16.80	-7.65	-14	40.89	-16.68	46	34.90	-14.95
-73	17.22	-7.88	-13	41.28	-16.79	47	34.40	-14.79
-72	17.63	-8.10	-12	41.68	-16.90	48	33.90	-14.63
-71	18.02	-8.30	-11	42.08	-17.01	49	33.38	-14.47
-70	18.40	-8.49	-10	42.43	-17.10	50	32.85	-14.30
-69	18.76	-8.67	-9	42.81	-17.20	51	32.32	-14.13
-68	19.04	-8.81	-8	43.18	-17.30	52	31.80	-13.95
-67	19.32	-8.95	-7	43.45	-17.37	53	31.30	-13.79
-66	19.56	-9.07	-6	43.75	-17.45	54	30.80	-13.62
-65	19.79	-9.18	-5	44.04	-17.52	55	30.30	-13.45
-64	20.01	-9.29	-4	44.33	-17.60	56	29.80	-13.27
-63	20.16	-9.36	-3	44.59	-17.67	57	29.30	-13.10
-62	20.31	-9.43	-2	44.81	-17.72	58	28.86	-12.94
-61	20.49	-9.51	-1	45.00	-17.77	59	28.43	-12.78
-60	20.70	-9.61	0	45.18	-17.82	60	28.00	-12.63
-59	20.91	-9.71	1	45.35	-17.86	61	27.55	-12.46
-58	21.13	-9.81	2	45.49	-17.90	62	27.09	-12.29
-57	21.34	-9.91	3	45.62	-17.93	63	26.64	-12.11
-56	21.56	-10.01	4	45.74	-17.96	64	26.22	-11.95
-55	21.81	-10.12	5	45.85	-17.99	65	25.82	-11.80
-54	22.07	-10.23	6	45.96	-18.01	66	25.42	-11.64
-53	22.33	-10.35	7	46.00	-18.02	67	25.03	-11.48
-52	22.64	-10.48	8	46.00	-18.02	68	24.66	-11.34
-51	22.95	-10.62	9	46.00	-18.02	69	24.30	-11.19
-50	23.28	-10.76	10	46.00	-18.02	70	23.94	-11.04
-49	23.63	-10.91	11	46.00	-18.02	71	23.61	-10.90
-48	23.98	-11.06	12	45.94	-18.01	72	23.29	-10.76
-47	24.34	-11.20	13	45.86	-17.99	73	22.96	-10.62
-46	24.77	-11.38	14	45.79	-17.97	74	22.64	-10.48
-45	25.19	-11.55	15	45.72	-17.95	75	22.31	-10.34
-44	25.62	-11.72	16	45.61	-17.93	76	21.99	-10.20
-43	26.08	-11.90	17	45.49	-17.90	77	21.67	-10.05
-42	26.55	-12.08	18	45.36	-17.86	78	21.32	-9.90
-41	27.02	-12.26	19	45.18	-17.82	79	20.98	-9.74
-40	27.49	-12.44	20	44.99	-17.77	80	20.63	-9.58
-39	27.98	-12.62	21	44.78	-17.72	81	20.28	-9.42
-38	28.46	-12.80	22	44.55	-17.66	82	19.93	-9.25
-37	28.95	-12.97	23	44.32	-17.60	83	19.57	-9.08
-36	29.49	-13.16	24	44.03	-17.52	84	19.15	-8.87
-35	30.02	-13.35	25	43.73	-17.44	85	18.72	-8.66
-34	30.56	-13.53	26	43.42	-17.36	86	18.29	-8.44
-33	31.11	-13.72	27	43.12	-17.28	87	17.83	-8.20
-32	31.67	-13.91	28	42.80	-17.20	88	17.36	-7.96
-31	32.22	-14.09	29	42.45	-17.10	89	16.90	-7.71

TABLE 1B. Venus latitude, right-looking incidence angle, and Muhleman correction in decibels. South latitudes are negative, north latitudes are positive.
[correction factor can be added to Magellan normalized cross section values to obtain backscatter coefficient σ_o]

Lat	Ang	Factor	Lat	Ang	Factor	Lat	Ang	Factor
-90	******	******	-30	25.14	-11.53	30	24.99	-11.47
-89	13.14	-5.49	-29	25.11	-11.51	31	25.00	-11.47
-88	13.49	-5.71	-28	25.08	-11.50	32	25.00	-11.47
-87	13.87	-5.95	-27	25.05	-11.49	33	25.00	-11.47
-86	14.31	-6.22	-26	25.02	-11.48	34	25.00	-11.47
-85	14.75	-6.49	-25	25.00	-11.47	35	25.00	-11.47
-84	15.25	-6.78	-24	25.00	-11.47	36	25.00	-11.47
-83	15.75	-7.07	-23	25.00	-11.47	37	25.00	-11.47
-82	16.23	-7.34	-22	25.00	-11.47	38	25.00	-11.47
-81	16.71	-7.60	-21	24.98	-11.46	39	25.00	-11.47
-80	17.24	-7.89	-20	24.95	-11.45	40	25.00	-11.47
-79	17.75	-8.16	-19	24.92	-11.44	41	25.00	-11.47
-78	18.24	-8.41	-18	24.90	-11.43	42	25.00	-11.47
-77	18.71	-8.65	-17	24.90	-11.43	43	25.00	-11.47
-76	19.14	-8.87	-16	24.90	-11.43	44	25.00	-11.47
-75	19.60	-9.09	-15	24.90	-11.43	45	25.00	-11.47
-74	20.08	-9.32	-14	24.88	-11.42	46	25.00	-11.47
-73	20.50	-9.52	-13	24.84	-11.41	47	25.00	-11.47
-72	20.88	-9.70	-12	24.81	-11.40	48	25.00	-11.47
-71	21.27	-9.87	-11	24.80	-11.39	49	25.00	-11.47
-70	21.63	-10.04	-10	24.80	-11.39	50	25.00	-11.47
-69	21.96	-10.18	-9	24.80	-11.39	51	25.00	-11.47
-68	22.24	-10.31	-8	24.80	-11.39	52	25.00	-11.47
-67	22.52	-10.43	-7	24.80	-11.39	53	25.00	-11.47
-66	22.81	-10.56	-6	24.80	-11.39	54	25.00	-11.47
-65	23.08	-10.67	-5	24.80	-11.39	55	25.00	-11.47
-64	23.33	-10.78	-4	24.80	-11.39	56	25.00	-11.47
-63	23.56	-10.88	-3	24.80	-11.39	57	25.00	-11.47
-62	23.75	-10.96	-2	24.80	-11.39	58	25.00	-11.47
-61	23.93	-11.04	-1	24.80	-11.39	59	25.00	-11.47
-60	24.10	-11.10	0	24.80	-11.39	60	25.00	-11.47
-59	24.25	-11.17	1	24.80	-11.39	61	25.00	-11.47
-58	24.40	-11.23	2	24.80	-11.39	62	25.00	-11.47
-57	24.53	-11.28	3	24.80	-11.39	63	25.00	-11.47
-56	24.63	-11.32	4	24.80	-11.39	64	25.00	-11.47
-55	24.72	-11.36	5	24.80	-11.39	65	25.00	-11.47
-54	24.81	-11.40	6	24.80	-11.39	66	25.00	-11.47
-53	24.88	-11.42	7	24.80	-11.39	67	25.00	-11.47
-52	24.94	-11.45	8	24.80	-11.39	68	25.00	-11.47
-51	25.00	-11.47	9	24.80	-11.39	69	24.96	-11.45
-50	25.06	-11.50	10	24.80	-11.39	70	24.92	-11.44
-49	25.12	-11.52	11	24.80	-11.39	71	24.90	-11.43
-48	25.19	-11.55	12	24.81	-11.39	72	24.90	-11.43
-47	25.20	-11.55	13	24.83	-11.40	73	24.89	-11.43
-46	25.20	-11.55	14	24.85	-11.41	74	24.80	-11.39
-45	25.20	-11.55	15	24.87	-11.42	75	24.70	-11.35
-44	25.20	-11.55	16	24.89	-11.43	76	*****	******
-43	25.20	-11.55	17	24.90	-11.43	77	*****	******
-42	25.20	-11.55	18	24.90	-11.43	78	*****	******
-41	25.20	-11.55	19	24.90	-11.43	79	*****	******
-40	25.20	-11.55	20	24.90	-11.43	80	*****	******
-39	25.20	-11.55	21	24.90	-11.43	81	*****	******
-38	25.20	-11.55	22	24.90	-11.43	82	*****	******
-37	25.20	-11.55	23	24.90	-11.43	83	*****	******
-36	25.20	-11.55	24	24.90	-11.43	84	*****	******
-35	25.20	-11.55	25	24.90	-11.43	85	*****	******
-34	25.20	-11.55	26	24.90	-11.43	86	*****	******
-33	25.20	-11.55	27	24.92	-11.44	87	*****	******
-32	25.20	-11.55	28	24.95	-11.45	88	*****	******
-31	25.17	-11.54	29	24.97	-11.46	89	*****	******

TABLE 1C. Venus latitude, special left-looking Maxwell profile incidence angle, and Muhleman correction in decibels. South latitudes are negative, north latitudes are positive.
[correction factor can be added to Magellan normalized cross section values to obtain backscatter coefficient σ_o]

Lat	Ang	Factor	Lat	Ang	Factor	Lat	Ang	Factor
-90	*****	******	-30	*****	******	30	33.10	-14.38
-89	*****	******	-29	*****	******	31	33.33	-14.45
-88	*****	******	-28	*****	******	32	33.55	-14.52
-87	*****	******	-27	*****	******	33	33.78	-14.59
-86	*****	******	-26	*****	******	34	33.99	-14.66
-85	*****	******	-25	*****	******	35	34.20	-14.73
-84	*****	******	-24	*****	******	36	34.40	-14.79
-83	*****	******	-23	*****	******	37	34.59	-14.85
-82	*****	******	-22	*****	******	38	34.77	-14.91
-81	*****	******	-21	*****	******	39	34.94	-14.96
-80	*****	******	-20	*****	******	40	35.11	-15.01
-79	*****	******	-19	*****	******	41	35.27	-15.06
-78	*****	******	-18	*****	******	42	35.42	-15.11
-77	*****	******	-17	*****	******	43	35.55	-15.14
-76	*****	******	-16	*****	******	44	35.67	-15.18
-75	*****	******	-15	*****	******	45	35.77	-15.21
-74	*****	******	-14	*****	******	46	35.86	-15.24
-73	*****	******	-13	*****	******	47	35.94	-15.26
-72	*****	******	-12	*****	******	48	36.00	-15.28
-71	*****	******	-11	*****	******	49	36.05	-15.30
-70	*****	******	-10	*****	******	50	36.08	-15.31
-69	*****	******	-9	*****	******	51	36.08	-15.31
-68	*****	******	-8	*****	******	52	36.06	-15.30
-67	*****	******	-7	*****	******	53	36.03	-15.29
-66	*****	******	-6	*****	******	54	35.98	-15.28
-65	*****	******	-5	*****	******	55	35.90	-15.25
-64	*****	******	-4	*****	******	56	35.78	-15.22
-63	*****	******	-3	*****	******	57	35.65	-15.18
-62	*****	******	-2	*****	******	58	35.48	-15.12
-61	*****	******	-1	*****	******	59	35.29	-15.07
-60	*****	******	0	*****	******	60	35.06	-15.00
-59	*****	******	1	*****	******	61	34.81	-14.92
-58	*****	******	2	*****	******	62	34.51	-14.82
-57	*****	******	3	*****	******	63	34.18	-14.72
-56	*****	******	4	*****	******	64	33.80	-14.60
-55	*****	******	5	*****	******	65	33.40	-14.47
-54	*****	******	6	*****	******	66	32.93	-14.33
-53	*****	******	7	*****	******	67	32.46	-14.17
-52	*****	******	8	*****	******	68	31.95	-14.00
-51	*****	******	9	*****	******	69	31.38	-13.81
-50	*****	******	10	*****	******	70	30.77	-13.61
-49	*****	******	11	*****	******	71	30.12	-13.38
-48	*****	******	12	*****	******	72	29.42	-13.14
-47	*****	******	13	*****	******	73	28.68	-12.87
-46	*****	******	14	*****	******	74	27.90	-12.59
-45	*****	******	15	*****	******	75	27.08	-12.28
-44	*****	******	16	*****	******	76	26.21	-11.95
-43	*****	******	17	*****	******	77	*****	******
-42	*****	******	18	*****	******	78	*****	******
-41	*****	******	19	30.32	-13.45	79	*****	******
-40	*****	******	20	30.59	-13.55	80	*****	******
-39	*****	******	21	30.85	-13.64	81	*****	******
-38	*****	******	22	31.12	-13.72	82	*****	******
-37	*****	******	23	31.37	-13.81	83	*****	******
-36	*****	******	24	31.63	-13.90	84	*****	******
-35	*****	******	25	31.88	-13.98	85	*****	******
-34	*****	******	26	32.13	-14.06	86	*****	******
-33	*****	******	27	32.38	-14.15	87	*****	******
-32	*****	******	28	32.62	-14.22	88	*****	******
-31	*****	******	29	32.86	-14.30	89	*****	******

TABLE 1D. Venus latitude, left-looking stereo incidence angle, and Muhleman correction in decibels. South latitudes are negative, north latitudes are positive.
[correction factor can be added to Magellan normalized cross section values to obtain backscatter coefficient σ_o]

Lat	Ang	Factor	Lat	Ang	Factor	Lat	Ang	Factor
-90	*****	******	-30	17.50	-8.03	30	23.90	-11.02
-89	*****	******	-29	17.76	-8.17	31	23.69	-10.93
-88	*****	******	-28	18.03	-8.30	32	23.46	-10.84
-87	*****	******	-27	18.29	-8.44	33	23.22	-10.74
-86	*****	******	-26	18.56	-8.57	34	22.98	-10.63
-85	*****	******	-25	18.83	-8.71	35	22.71	-10.52
-84	*****	******	-24	19.10	-8.84	36	22.44	-10.40
-83	*****	******	-23	19.38	-8.98	37	22.17	-10.28
-82	*****	******	-22	19.65	-9.11	38	21.89	-10.16
-81	*****	******	-21	19.93	-9.25	39	21.61	-10.03
-80	*****	******	-20	20.20	-9.38	40	21.31	-9.89
-79	*****	******	-19	20.46	-9.50	41	21.00	-9.75
-78	*****	******	-18	20.73	-9.63	42	20.68	-9.60
-77	*****	******	-17	21.00	-9.75	43	20.36	-9.45
-76	11.55	-4.43	-16	21.26	-9.87	44	20.04	-9.30
-75	11.96	-4.71	-15	21.52	-9.99	45	19.73	-9.15
-74	12.37	-4.98	-14	21.77	-10.10	46	19.40	-8.99
-73	12.69	-5.20	-13	22.03	-10.22	47	18.94	-8.77
-72	12.94	-5.36	-12	22.27	-10.32	48	18.70	-8.64
-71	13.14	-5.49	-11	22.52	-10.43	49	18.39	-8.49
-70	13.34	-5.62	-10	22.74	-10.53	50	18.06	-8.32
-69	13.45	-5.69	-9	22.98	-10.63	51	17.72	-8.15
-68	13.56	-5.76	-8	23.21	-10.73	52	17.39	-7.97
-67	13.63	-5.80	-7	23.42	-10.82	53	17.06	-7.79
-66	13.69	-5.84	-6	23.62	-10.90	54	16.75	-7.63
-65	13.71	-5.85	-5	23.81	-10.99	55	16.44	-7.46
-64	13.73	-5.86	-4	24.00	-11.06	56	16.13	-7.28
-63	13.73	-5.86	-3	24.19	-11.14	57	15.84	-7.12
-62	13.73	-5.86	-2	24.36	-11.21	58	15.55	-6.96
-61	13.72	-5.86	-1	24.53	-11.28	59	15.28	-6.80
-60	13.71	-5.85	0	24.68	-11.34	60	15.02	-6.65
-59	13.70	-5.85	1	24.82	-11.40	61	14.77	-6.50
-58	13.70	-5.85	2	24.95	-11.45	62	14.54	-6.36
-57	13.70	-5.85	3	25.08	-11.50	63	14.33	-6.23
-56	13.71	-5.85	4	25.19	-11.55	64	14.13	-6.11
-55	13.72	-5.86	5	25.28	-11.59	65	13.96	-6.01
-54	13.75	-5.88	6	25.37	-11.62	66	13.80	-5.91
-53	13.78	-5.90	7	25.45	-11.65	67	13.66	-5.82
-52	13.83	-5.92	8	25.52	-11.68	68	13.55	-5.75
-51	13.88	-5.96	9	25.58	-11.70	69	13.45	-5.69
-50	13.95	-6.00	10	25.63	-11.72	70	13.39	-5.65
-49	14.03	-6.05	11	25.65	-11.73	71	13.34	-5.62
-48	14.10	-6.10	12	25.67	-11.74	72	13.32	-5.61
-47	14.21	-6.16	13	25.67	-11.74	73	13.32	-5.61
-46	14.32	-6.23	14	25.68	-11.74	74	13.34	-5.62
-45	14.44	-6.30	15	25.65	-11.73	75	13.38	-5.64
-44	14.58	-6.39	16	25.63	-11.72	76	13.44	-5.68
-43	14.72	-6.47	17	25.58	-11.70	77	13.50	-5.72
-42	14.89	-6.57	18	25.53	-11.68	78	13.58	-5.77
-41	15.06	-6.67	19	25.46	-11.66	79	13.67	-5.83
-40	15.24	-6.77	20	25.38	-11.62	80	13.74	-5.87
-39	15.43	-6.88	21	25.28	-11.59	81	13.82	-5.92
-38	15.63	-7.00	22	25.18	-11.54	82	13.87	-5.95
-37	15.84	-7.12	23	25.06	-11.50	83	13.91	-5.97
-36	16.05	-7.24	24	24.93	-11.44	84	13.89	-5.96
-35	16.28	-7.37	25	24.79	-11.39	85	13.82	-5.92
-34	16.51	-7.49	26	24.63	-11.32	86	13.67	-5.83
-33	16.74	-7.62	27	24.48	-11.26	87	13.41	-5.66
-32	16.99	-7.75	28	24.29	-11.18	88	12.67	-5.18
-31	17.24	-7.89	29	24.10	-11.10	89	*****	*****

TABLE 2. Example Venus geologic map data tables.
[Values for these three sites were obtained using the mgn_data and anc_data programs, whose output is presented in app. 1 and 2. The first table presents information on image location, pixel scale (Δ), number of pixels used in the backscatter calculation (N), range of incidence angles, and radius. The second table provides the backscatter and physical properties data: backscatter cross section (σ_o), rms slope (θ_{rms}), Fresnel reflectivity (ρ), emissivity, and calculated dielectric constants for the smooth-surface (ε_s) and rough-surface (ε_r) cases discussed in the text. Note that latitude, longitude boundaries are listed in both the body of the unit description and here. For the backscatter cross section, values in parentheses represent the σ_o value (in dB) at plus and minus one standard deviation. For all other data, values in parentheses represent the minimum and maximum values of each parameter within the chosen sample box. The number of significant digits used for each value are reasonable guides to their accuracy]

Unit	Lat, Lon	Δ	N	Angle (deg)	Radius (range) in km
p1	30.863-30.999 N; 43.502-43.666 E	225 m	4290	41.7-41.8	6051.540 (6051.508, 6051.551)
f1	30.418-30.465 N; 43.495-43.568 E	225 m	690	41.9-41.9	6051.421 (6051.399, 6051.452)
f2	30.637-30.746 N; 43.842-44.030 E	225 m	3952	41.8-41.9	6051.493 (6051.484, 6051.504)

Unit	σ_o (dB)	θ_{rms} (deg)	ρFresnel	Emissivity	ε_s, ε_r
p1	-18.14 (-19.40, -17.17)	1.6 (1.4, 1.9)	0.114 (0.085, 0.145)	0.828 (0.819, 0.840)	3.7, 5.6
f1	-7.80 (-8.91, -6.91)	4.3 (3.6, 4.9)	0.093 (0.080, 0.100)	0.856 (0.849, 0.864)	3.2, 4.7
f2	-11.20 (-12.52, -10.19)	4.6 (3.0, 7.4)	0.100 (0.085, 0.120)	0.846 (0.840, 0.854)	3.4, 5.0

TABLE 3. Values of horizontal-polarization emissivity and corresponding dielectric constants of plane and rough surfaces at five incidence (emission) angles.
[Left-hand columns are smooth plane-surface estimates, right-hand columns are for rough surfaces. The rows that bracket the planetary mean value of 0.845 are shown in bold-face type]

Emis.	25°		30°		35°		40°		45°	
0.50	28.09	34.09	25.73	34.21	23.13	34.43	20.35	34.80	17.49	35.39
0.51	26.56	32.21	24.34	32.33	21.88	32.53	19.26	32.85	16.56	33.38
0.52	25.13	30.46	23.03	30.56	20.71	30.74	18.24	31.03	15.69	31.50
0.53	23.79	28.82	21.81	28.91	19.62	29.07	17.28	29.32	14.87	29.74
0.54	22.53	27.28	20.66	27.36	18.59	27.49	16.38	27.72	14.11	28.09
0.55	21.35	25.83	19.58	25.90	17.62	26.02	15.54	26.22	13.39	26.54
0.56	20.23	24.47	18.56	24.53	16.71	24.63	14.74	24.81	12.71	25.08
0.57	19.18	23.18	17.60	23.24	15.86	23.33	13.99	23.48	12.07	23.71
0.58	18.20	21.97	16.70	22.02	15.05	22.10	13.29	22.23	11.47	22.43
0.59	17.27	20.84	15.85	20.87	14.29	20.94	12.62	21.05	10.90	21.21
0.60	16.39	19.76	15.05	19.79	13.57	19.85	11.99	19.93	10.37	20.07
0.61	15.56	18.74	14.29	18.77	12.89	18.81	11.40	18.88	9.86	18.99
0.62	14.77	17.78	13.58	17.80	12.25	17.84	10.84	17.89	9.39	17.98
0.63	14.03	16.87	12.90	16.89	11.64	16.91	10.31	16.96	8.93	17.02
0.64	13.33	16.01	12.26	16.02	11.07	16.04	9.81	16.07	8.51	16.11
0.65	12.66	15.20	11.65	15.20	10.53	15.21	9.33	15.23	8.10	15.25
0.66	12.03	14.43	11.07	14.43	10.01	14.43	8.88	14.43	7.71	14.44
0.67	11.43	13.69	10.52	13.69	9.52	13.69	8.45	13.68	7.35	13.66
0.68	10.86	13.00	10.00	12.99	9.05	12.98	8.04	12.97	7.00	12.93
0.69	10.32	12.34	9.51	12.33	8.61	12.31	7.66	12.29	6.67	12.24
0.70	9.80	11.71	9.04	11.70	8.19	11.68	7.29	11.64	6.36	11.58
0.71	9.31	11.11	8.59	11.10	7.79	11.07	6.94	11.03	6.06	10.96
0.72	8.85	10.54	8.17	10.52	7.41	10.50	6.61	10.45	5.78	10.37
0.73	8.40	10.00	7.76	9.98	7.05	9.95	6.29	9.90	5.51	9.81
0.74	7.98	9.48	7.37	9.46	6.70	9.43	5.99	9.37	5.25	9.27
0.75	7.58	8.99	7.01	8.97	6.37	8.93	5.70	8.87	5.01	8.76
0.76	7.19	8.52	6.65	8.49	6.06	8.46	5.42	8.39	4.77	8.28
0.77	6.82	8.07	6.32	8.04	5.76	8.00	5.16	7.93	4.55	7.81
0.78	6.47	7.64	6.00	7.61	5.47	7.57	4.91	7.50	4.33	7.37
0.79	6.14	7.23	5.69	7.20	5.20	7.16	4.67	7.08	4.13	6.95
0.80	5.81	6.84	5.40	6.81	4.93	6.76	4.44	6.68	3.93	6.55
0.81	5.51	6.46	5.11	6.43	4.68	6.39	4.22	6.31	3.74	6.17
0.82	5.21	6.10	4.84	6.07	4.44	6.03	4.01	5.94	3.56	5.81
0.83	4.93	5.76	4.59	5.73	4.21	5.68	3.81	5.60	3.39	5.46
0.84	**4.66**	**5.43**	**4.34**	**5.40**	**3.99**	**5.35**	**3.61**	**5.26**	**3.23**	**5.13**
0.85	**4.39**	**5.11**	**4.10**	**5.08**	**3.77**	**5.03**	**3.43**	**4.95**	**3.07**	**4.81**
0.86	4.14	4.80	3.87	4.77	3.57	4.73	3.25	4.64	2.92	4.50
0.87	3.90	4.51	3.65	4.48	3.37	4.43	3.07	4.35	2.77	4.21
0.88	3.67	4.23	3.44	4.20	3.18	4.15	2.91	4.07	2.63	3.93
0.89	3.44	3.95	3.23	3.93	3.00	3.88	2.75	3.80	2.49	3.66
0.90	3.23	3.69	3.03	3.66	2.82	3.61	2.59	3.54	2.36	3.41
0.91	3.02	3.43	2.84	3.41	2.65	3.36	2.44	3.28	2.23	3.16
0.92	2.81	3.18	2.65	3.16	2.48	3.12	2.30	3.04	2.10	2.92
0.93	2.61	2.94	2.47	2.92	2.32	2.88	2.15	2.80	1.98	2.69
0.94	2.42	2.70	2.29	2.68	2.16	2.64	2.01	2.57	1.86	2.47
0.95	2.22	2.47	2.12	2.45	2.00	2.41	1.88	2.35	1.75	2.25
0.96	2.03	2.24	1.94	2.22	1.84	2.19	1.74	2.13	1.63	2.04
0.97	1.84	2.00	1.77	1.99	1.69	1.96	1.60	1.91	1.51	1.83
0.98	1.64	1.76	1.58	1.75	1.52	1.72	1.46	1.68	1.39	1.61
0.99	1.41	1.49	1.38	1.48	1.34	1.46	1.29	1.43	1.25	1.38

TABLE 4. Fresnel reflectivity (reflection coefficient at zero incidence angle) and the corresponding dielectric constant.

Reflectivity	Dielectric Constant	Reflectivity	Dielectric Constant
0.01	1.49	0.51	35.96
0.02	1.77	0.52	38.08
0.03	2.01	0.53	40.36
0.04	2.25	0.54	42.81
0.05	2.48	0.55	45.43
0.06	2.72	0.56	48.26
0.07	2.96	0.57	51.30
0.08	3.20	0.58	54.59
0.09	3.45	0.59	58.14
0.10	3.71	0.60	61.98
0.11	3.97	0.61	66.15
0.12	4.24	0.62	70.68
0.13	4.53	0.63	75.62
0.14	4.82	0.64	81.00
0.15	5.13	0.65	86.89
0.16	5.44	0.66	93.34
0.17	5.78	0.67	100.43
0.18	6.12	0.68	108.24
0.19	6.48	0.69	116.87
0.20	6.85	0.70	126.44
0.21	7.25	0.71	137.07
0.22	7.66	0.72	148.93
0.23	8.08	0.73	162.21
0.24	8.53	0.74	177.14
0.25	9.00	0.75	193.99
0.26	9.49	0.76	213.11
0.27	10.01	0.77	234.89
0.28	10.55	0.78	259.85
0.29	11.11	0.79	288.62
0.30	11.71	0.80	322.00
0.31	12.34	0.81	361.00
0.32	13.00	0.82	406.94
0.33	13.69	0.83	461.51
0.34	14.42	0.84	527.00
0.35	15.19	0.85	606.44
0.36	16.00	0.86	704.04
0.37	16.86	0.87	825.67
0.38	17.76	0.88	979.78
0.39	18.72	0.89	1178.86
0.40	19.73	0.90	1442.00
0.41	20.80	0.91	1799.53
0.42	21.93	0.92	2302.00
0.43	23.13	0.93	3038.73
0.44	24.41	0.94	4179.77
0.45	25.76	0.95	6081.99
0.46	27.20	0.96	9601.98
0.47	28.74	0.97	17246.52
0.48	30.37	0.98	39202.24
0.49	32.11		
0.50	33.97		

APPENDIX 1

Calculation of Backscatter Coefficients from Magellan Images Using the MGN_DATA Program

1. Obtain the program by anonymous ftp from ceps.nasm.edu (192.138.170.27). The material is in /pub/venus. The ftp directory contains the source code, mgn_data.f, along with a compiled version made using the static options to allow the code to run on machines that do not have Fortran installed. This program was set up on a Sun Sparc workstation but should be VAX-compatible with some adjustments to the read statements that access the CD-ROM.

2. Compile the program on your machine using [f77 -e -o mgn_data mgn_data.f], or just use the already compiled version if your machine will accept it.

3. Mount a CD-ROM with the desired image product.

5. Using whatever display program you choose, set up one of the framelets such that you can read the (x,y) pixel locations of points within the image.

6. From the CD-ROM directory of the chosen MIDR, run the compiled program in a separate window.

7. The program will ask for (a) a destination file path and name for the output log file, (b) what type of incidence angle profile this image used, (c) whether this is a C-MIDR or F-MIDR, and (d) the name of the framelet label file you want to work with. Version 2 of this program now permits all four DLAP modes to be selected (left, right, stereo, Maxwell).

8. Once it gets the mapping information from the image header, the program allows you to select corner points of boxes within the framelet. It will then report the (latitude, longitude) boundaries of the box, the range of incidence angles, and the mean and standard deviation of all non-zero pixels. The output average echo is in backscatter cross section per unit area (backscatter coefficient) and has had the Muhleman correction taken out. The values in parentheses following the mean echo, in decibels, are the coefficients at plus and minus one standard deviation, also in decibels.

For each box you may also add a one-line annotation to indicate the terrain type on the log file.

A sample run of the program and its output follows.

EXAMPLE OF A SESSION WITH MGN_DATA

```
/cdrom/c130n045: 3>mgn_data
Name of the data log file (in single quotes)?
'/home/campbell/guide/logfile'
Input label file from a Magellan CD-ROM?
c1f28.lbl
 Specify DLAP for this image:
 Left-looking: l
 Right-looking: r
 Cycle 3 Maxwell: m
 Stereo: s
l
 Is this an F-MIDR or a C-MIDR (c or f)?
c
Upper left (x,y) and lower right (x,y) of box?
248,18,313,82
Description of site for log file (s. quotes)?
'Plains Unit 1'
 Box coordinates:
Upper left lat, lon:                30.99926        43.50247
Upper right lat, lon:               30.99926        43.66403
Lower left lat, lon:                30.86304        43.50522
Lower right lat, lon:               30.86304        43.66654
Range of angle across the box: 41.71  41.76
 Number of non-zero points in box:    4290
Mean and standard deviation of SAR: 0.0153   0.0039
Mean SAR echo in decibels: -18.140  (-19.397, -17.166)
 Would you like another box?
y
 Upper left (x,y) and lower right (x,y) of box? 241,269,270,291
 Description of site for log file (s. quotes)?
'Bright Lava Flow'
 Box coordinates:
Upper left lat, lon:                30.46505        43.49583
Upper right lat, lon:               30.46505        43.56751
Lower left lat, lon:                30.41822        43.49676
Lower right lat, lon:               30.41822        43.56841
Range of angle across the box: 41.92  41.94
 Number of non-zero points in box:     690
Mean and standard deviation of SAR: 0.1660   0.0376
Mean SAR echo in decibels:  -7.799  ( -8.914,  -6.912)
 Would you like another box?
y
 Upper left (x,y) and lower right (x,y) of box? 383,137,458,188
 Description of site for log file (s. quotes)?
'Moderate Lava Flow'
 Box coordinates:
Upper left lat, lon:                30.74599        43.84222
Upper right lat, lon:               30.74599        44.02813
Lower left lat, lon:                30.63744        43.84400
Lower right lat, lon:               30.63744        44.02971
Range of angle across the box: 41.81  41.85
 Number of non-zero points in box:    3952
Mean and standard deviation of SAR: 0.0758   0.0199
Mean SAR echo in decibels: -11.202  (-12.522, -10.191)
 Would you like another box?
n
```

OUTPUT OF MGN_DATA RUN

Data from Magellan Image Framelet: C1F28.IMG
Part of Magellan Image: C1-MIDR.30N045;201
Pixel scale of image (m): 225.000

Plains Unit
Box pixel boundaries (x1,y1,x2,y2): 248 18 313 82
Box coordinates:

Upper left lat, lon:	30.99926	43.50247
Upper right lat, lon:	30.99926	43.66403
Lower left lat, lon:	30.86304	43.50522
Lower right lat, lon:	30.86304	43.66654

Range of angle across the box: 41.71 41.76
Number of non-zero points in box: 4290
Mean and standard deviation of SAR: 0.0153 0.0039
Mean SAR echo in decibels: -18.140 (-19.397, -17.166)

Bright Lava Flow
Box pixel boundaries (x1,y1,x2,y2): 241 269 270 291
Box coordinates:

Upper left lat, lon:	30.46505	43.49583
Upper right lat, lon:	30.46505	43.56751
Lower left lat, lon:	30.41822	43.49676
Lower right lat, lon:	30.41822	43.56841

Range of angle across the box: 41.92 41.94
Number of non-zero points in box: 690
Mean and standard deviation of SAR: 0.1660 0.0376
Mean SAR echo in decibels: -7.799 (-8.914, -6.912)

Moderate Lava Flow
Box pixel boundaries (x1,y1,x2,y2): 383 137 458 188
Box coordinates:

Upper left lat, lon:	30.74599	43.84222
Upper right lat, lon:	30.74599	44.02813
Lower left lat, lon:	30.63744	43.84400
Lower right lat, lon:	30.63744	44.02971

Range of angle across the box: 41.81 41.85
Number of non-zero points in box: 3952
Mean and standard deviation of SAR: 0.0758 0.0199
Mean SAR echo in decibels: -11.202 (-12.522, -10.191)

APPENDIX 2

Calculating Average Values of Ancillary Data with the ANC_DATA Program

The Fortran program **anc_data** will provide average values and ranges for elevation, rms slope, emissivity, and Fresnel reflectivity. Smooth and rough-surface dielectric constants, discussed in the text, are also calculated. The only inputs to the program are latitude and longitude coordinates for a sample box. Data values are taken from cylindrical projection files of the maps on GxDR Volume 2 (a mosaic of the Mercator and polar stereo maps in each directory), which you need to copy from the public ftp account on ceps.nasm.edu. File names are emis.cyl, rms.cyl, refl.cyl, and topo.cyl, which in total occupy 200 Mbytes of disk space. The program should be run in whatever directory you place these data files. The resolution of the reprojected maps is 0.044° per pixel. A sample run and output are shown below.

```
/home/campbell/guide: 236>anc_data
 Output log file name?
'logfile2'
 Lat Range (S, N), Long Range (W, E)?
30.863,30.999,43.502,43.666
 Would you like another box (y or n)?
y
 Lat Range (S, N), Long Range (W, E)?
30.418,30.465,43.495,43.568
 Would you like another box (y or n)?
y
 Lat Range (S, N), Long Range (W, E)?
30.637,30.746,43.842,44.030
 Would you like another box (y or n)?
n
```

OUTPUT FILE:

```
Lat, Long Box: [( 30.863,  30.999), ( 43.502,  43.666)]
Mean and Range (min, max) of Physical Properties:
Elevation (km):   6051.540  (6051.508, 6051.551)
RMS slope (deg):  1.57  ( 1.40,  1.90)
Fresnel Reflectivity: .114  (.085, .145)
Emissivity: .828  (.819, .840)
Incidence angle (deg): 42.
Smooth and Rough-Surface Diel. Values: 3.7, 5.6

Lat, Long Box: [( 30.418,  30.465), ( 43.495,  43.568)]
Mean and Range (min, max) of Physical Properties:
Elevation (km):   6051.421  (6051.399, 6051.452)
RMS slope (deg):  4.28  ( 3.60,  4.90)
Fresnel Reflectivity: .093  (.080, .100)
Emissivity: .856  (.849, .864)
Incidence angle (deg): 42.
Smooth and Rough-Surface Diel. Values: 3.2, 4.7

Lat, Long Box: [( 30.637,  30.746), ( 43.842,  44.030)]
Mean and Range (min, max) of Physical Properties:
Elevation (km):   6051.493  (6051.484, 6051.504)
RMS slope (deg):  4.62  ( 3.00,  7.40)
Fresnel Reflectivity: .100  (.085, .120)
Emissivity: .846  (.840, .854)
Incidence angle (deg): 42.
Smooth and Rough-Surface Diel. Values: 3.4, 5.0
```

APPENDIX 3
Useful Programs and Data Files

This section lists some other programs and data files available from ceps.nasm.edu over anonymous ftp. The source files can be compiled as described in appendix 1 or run directly from the executables provided in the ftp directory. For any questions or problems, contact Bruce Campbell (campbell@ceps.nasm.edu). The output of all mosaicking programs are simple 8-bit raster files with no header information, but the mapping data can be recovered from the framelet headers on the CD-ROM.

The ascii data files are for use in creating radar correlation charts for Venus backscatter data. The terrestrial AIRSAR data do not have error values listed with them, because the standard deviations vary with the degree of multilook averaging. Typical errors are about ±1 dB for these measurements. All backscatter coefficients are HH polarization interpolated 12.6-cm values derived from 6- and 24-cm data (eq. 4). See Campbell et al. [1993] for a discussion of the surface texture on these lava flows.

PROGRAMS:

midr.f --- Fortran program which mosaics all or some of the 56 tiles of an F, C1, C2, or C3 MIDR image directly from the CD-ROM. Prompts for destination file name and the tile coordinates (1-8 left to right; 1-7 top to bottom).

fmap.f --- A developmental Fortran program which mosaics and shrinks the FMAP tiles from a CD-rom to 150 m resolution. The resulting mosaic is about 8000 pixels square, which is typically a good size for filmwriters. The output map lower left corner corresponds to the edge of the lower left fmap tile. All other sides have some padding.

DATA FILES:

muhl.law --- ascii data file of incidence angle (column 1) and backscatter coefficient in decibels (column 2) for the average behavior of Venus derived by Muhleman [1964]. This backscatter law is the correct one proposed by Muhleman; note that the coefficients used in the Magellan data processing are slightly different.

hh.1920aa.s --- ascii file of incidence angle versus backscatter coefficient (dB) for the 1920 a'a lava flow from Mauna Iki on Kilauea volcano.

hh.miaa.s --- ascii file of incidence angle versus backscatter coefficient (dB) for an a'a lava flow near the summit of Mauna Iki.

hh.1920pah.s --- ascii file of incidence angle versus backscatter coefficient (dB) for the 1920 pahoehoe lava flow from Mauna Iki.

hh.cald.s --- ascii file of incidence angle versus backscatter coefficient (dB) for the large pahoehoe flows on the floor of Kilauea Caldera, Hawaii.

hh.pond.s --- ascii file of incidence angle versus backscatter coefficient (dB) for the very smooth lava flows ponded in the floors of Halemaumau and Kilauea Iki craters, Hawaii.

APPENDIX 4
How to Obtain GIPS and MGMDQE

GIPS, an excellent package for manipulating Magellan image data, is available through the licensing office at MIT for a minimal cost. Write to:
Peter Richards
MIT Technology Licensing
Bldng. E32-300
Cambridge, MA 02142-1324

MGMDQE is available over the Internet from MIT, and the ARCDR CD-ROM's contain useful software as well (from the /software directory on an ARCDR):

a program called ARCDRLST which generates ASCII listings of selected ARCDR fields. This program is described in the ARCDRLST.TXT file.

a subroutine library called MGMLIB whose routines can be called by higher-level user-written software to read, write, and update binary data records and fields. They are documented in the MGMLIB.TXT file, which is also present as a UNIX manual file in MGMLIB.MAN.

NOTE: there exists a public domain software package called MGMDQE that displays ARCDR data files on Sun SPARCstations using the SunView interface. This code will also execute under the OpenWindows interface, but it is NOT a true X Window application. Internet users can copy it via anonymous ftp from the "delcano.mit.edu" server [18.75.0.80] in the file named "mgn/bin/mgmdqe.vvvv.sparc.tar.Z", where "vvvv" represents the latest version number. This file should be copied in BINARY mode.